Exact solutions for the resonant response of multiplets undergoing stochastic modulation

E. van Faassen
Department of Molecular Biophysics, Buys Ballot Laboratory, Utrecht State University, P.O. Box 80 000, 3508 TA Utrecht, The Netherlands
(Received 8 March 1991)

Line-shape analysis of transitions in a quantum system is a method widely applied to study relaxation processes on a microscopic scale. In many practical cases, this relaxation arises from stochastic modulation of the Hamiltonian due to interactions with a surrounding heat bath. Using a separable class of stochastic operators, the line-shape problem for a Hamiltonian with a single transition has been solved in closed form. This method is not appropriate for more complicated Hamiltonians with closely spaced multiplets, as the modulation may lead to significant coupling between the individual transitions in the multiplet. In this work, therefore, an investigation of the response function of a modulated multiplet is undertaken. The dynamical equation is derived from the stochastic Liouville equation for the density matrix. It is solved rigorously for two practical examples drawn from magnetic-resonance spectroscopy. These exact results are used to investigate the accuracy of approximations found in the literature.

PACS number(s): 32.70.Jz, 33.25.Bn, 33.35.Ex

I. INTRODUCTION

The study of the linear response of dynamical systems provides information on the system's internal structure as well as on its internal relaxation processes: The first determines its resonant behavior, whereas the latter determine the precise form of the resonant line shape. Many experimental studies of relaxation processes therefore employ line-shape analysis. Of the abundance of examples we mention the propagation of electromagnetic waves in random media [1], light scattering on particles in liquids [2], magnetic-resonance-absorption spectroscopy [3], phase noise in lasers [4], Kerr-effect relaxation [5], and electronics [6]. The resonant character of the dynamical response of such systems often allows a formulation in terms of harmonic oscillators, the frequencies of which are continuously modulated by the relaxation processes. For those cases where the relaxation is induced by random frequency fluctuations of Markovian nature, Kubo [7] formulated an equation of motion for the probability distribution function of the modulated process, from which physical observables may be subsequently computed. For a nonrelativistic quantum system it is commonly called the stochastic Liouville equation (SLE). This has found its widest application in the fields of magnetic-resonance and optical spectroscopy. Except for the limiting cases of very slow or very fast fluctuations (rigid-limit and Redfield regimes, respectively) where good approximations exist, the SLE is difficult to solve and has been conventionally treated with eigenfunction expansions [8-10]. However, these methods require a considerable numerical effort and lack the theoretical justification for such expansions (indeed, counterexamples can easily be constructed). Moreover, numerical problems are unavoidable for slow modulation, as the eigenvalues become dense. These problems motivated the author to introduce relaxation operators of separable form and to solve the SLE by algebraic rather than eigenfunction methods. Of crucial practical importance is the possibility of modeling even complicated relaxation processes with separable stochastic operators of very low rank.

In a previous paper [11] this method was applied to a modulated two-level system. This simple structure admitted reduction of the SLE to the equation of motion of a single harmonic oscillator undergoing frequency modulation. Many spectroscopic applications, however, involve the response of multiplets with several observable transitions. These may be sufficiently close as to be mixed by the modulation process. In that case the full problem in solving several coupled oscillators needs to be addressed. A physical realization of great practical importance is found in magnetic-resonance transitions in the presence of anisotropic hyperfine interactions (as they arise in nitroxide spin-probe spectroscopy, for example).

These complications have been recognized a long time ago and their implications studied within the framework of eigenfunction expansions. We will readdress this problem here with the approach based on separable dynamics, where the analytical and numerically rigorously stable solutions admit a clear view of the effects due to state mixing. Although we formulate the problem in terms of the familiar hyperfine couplings, we stress the applicability of the method to more general cases with stochastic state mixing.

In Sec. II we will present the dynamical equation for the linear response of a randomly tumbling paramagnetic particle with anisotropic hyperfine coupling to nuclear-spin degrees of freedom. The stochastic operator will be chosen of the simplest rank-one separable form and the system of coupled equations will be solved in close form for two special cases. The first case of a spin-$\frac{1}{2}$, nuclear-spin-$\frac{1}{2}$ system will be presented in Sec. III. The case of spin-1 and arbitrary nuclear spin will be treated in Sec. IV. Section V is devoted to a detailed study of the singularities of the response functions in the complex frequency plane. Special attention will be given to the effects caused by state mixing. The exact solutions obtained ad-

mit a study of the consequences of approximations found in the literature. A final section provides conclusions and suggestions for further application, followed by two appendixes providing some details on more technical algebraic manipulations.

II. REDUCED EQUATION OF MOTION

In a previous [11] paper we derived exact expressions for the response of a modulated simple two-level system without internal degrees of freedom. We assumed validity of the high-field approximation, which allowed identification of the spin quantum number as a conserved quantity of the Hamiltonian of the particle under consideration. This property admitted a total factorization of the coupled equations of motion into a complete set of decoupled scalar equations. The latter were individually solved with a suitable separable stochastic operator describing the modulation process. For systems with a more complicated structure, like coupling to internal degrees of freedom, such a decomposition will not necessarily occur. A prime example is given by the hyperfine coupling in magnetic resonance. Since Hamiltonians for realistic cases are dominated by the electronic Zeeman interaction with anisotropies of about a percent, the electronic spin quantum number is conserved to within a very good approximation. As the nuclear Zeeman term usually is much smaller, the nuclear-spin quantum number may not be conserved under the modulation process: For practical cases the hyperfine coupling is strongly anisotropic and relaxation processes like molecular tumbling will induce non-negligible mixing of the nuclear-spin states.

We therefore consider the linear response of a single isolated paramagnetic multiplet to a microwave probe field. In a nonrelativistic formulation its Hamiltonian is written as the sum of an electron Zeeman and hyperfine coupling term (we neglect the very small nuclear Zeeman contribution)

$$H(\Omega)=\mathbf{H}_0\cdot\mathsf{g}(\Omega)\cdot\hbar\mathbf{S}-\hbar\mathbf{S}\cdot\mathsf{A}(\Omega)\cdot\mathbf{I}\ , \tag{1}$$

where $\hbar\mathbf{S}$ and $\hbar\mathbf{I}$ are the electronic and nuclear-spin operators, respectively, satisfying the usual canonical commutation relations $[S_i,S_j]=i\epsilon_{ijk}S_k$ (idem for $\mathbf{I}$). The dominant Zeeman term is proportional to the external static magnetic field $\mathbf{H}_0$. Both the gyromagnetic and hyperfine tensors g and A account for anisotropy in the magnetic interactions as they have dependence on the orientation Ω of the particle with respect to the magnetic field. Being symmetric, each tensor should assume a diagonal form in some frame of reference. We make the usual assumption that a single molecular frame exists where both tensors diagonalize at the same time. We then specify the molecular orientation through the three Euler angles $\Omega=(\alpha,\beta,\gamma)$ which rotate the laboratory frame to the diagonalizing molecular frame. Let the diagonal forms of the coupling tensors be labeled with a subscript d. Then, in the laboratory frame, the coupling tensors acquire the usual rank-two dependence on Ω (in the conventions of Ref. [12])

$$\mathsf{g}(\Omega)=R(\Omega)\mathsf{g}_dR^{-1}(\Omega)\ , \tag{2a}$$

$$\mathsf{A}(\Omega)=R(\Omega)\mathsf{A}_dR^{-1}(\Omega)\ , \tag{2b}$$

$$R(\Omega)=e^{-i\alpha J_z}e^{-i\beta J_y}e^{-i\gamma J_z}\ . \tag{3}$$

For practical cases the anisotropy in the dominant Zeeman term is less than a percent. This makes the projection of the electron spin along the magnetic field $\mathbf{H}_0$ a nearly conserved quantity. In the laboratory frame we choose this direction as the z axis: $\mathbf{H}_0=H_0\hat{\mathbf{e}}_z$. Neglecting the nonsecular terms $\sim S_x$ and S_y (high-field approximation) as before, the Hamiltonian takes a form in which the spin and nuclear-spin degrees of freedom are factorized:

$$\begin{aligned}H(\Omega)&\approx S_z\otimes\hbar[\omega(\Omega)-\mathbf{a}(\Omega)\cdot\mathbf{I}]\\&=S_z\otimes\hat{H}(\Omega)\ ,\end{aligned} \tag{4}$$

where the second line defines the reduced Hamiltonian $\hat{H}$ in the space of nuclear-spin states. It is again a Hermitian operator. The orientation-dependent, reduced splittings are defined as

$$\omega(\Omega)\equiv|\hat{H}_0|\hat{\mathbf{e}}_z\cdot\mathsf{g}(\Omega)\cdot\hat{\mathbf{e}}_z\ , \tag{5}$$

$$\mathbf{a}(\Omega)\equiv\hat{\mathbf{e}}_z\cdot\mathsf{A}(\Omega)\ . \tag{6}$$

It should be noted that the three-component object $\mathbf{a}(\Omega)$ does not transform under rotations in the usual vectorial sense but rather as a row of a rank-two Cartesian tensor [cf. Eq. (2b)]. For example, $\mathbf{a}$ loses any Ω dependence if the hyperfine coupling is taken to be isotropic.

The time evolution of any physical observable may be computed from the density matrix. In the presence of stochastic modulation, the equation of motion for the density matrix is commonly called the SLE [7,13]. In the linear-response regime (nonsaturating microwave powers) it is sufficient to consider the deviation $\rho(\Omega,t)$ of the density matrix from its equilibrium value. For compactness we will refer to this deviation ρ as the density matrix as well. For this quantity the SLE takes the following form [11]:

$$\dot{\rho}=\frac{i}{\hbar}[\rho,H(\Omega)]-\Gamma\rho+2\kappa S_x\cos\omega_0t\ . \tag{7}$$

On the right-hand side, the commutator accounts for the free-Hamiltonian time propagation of the particle. The final harmonic driving term accounts for the electron-spin transitions induced by the transverse microwave probe field of strength κ and frequency ω_0. Power absorption of this field is the usual experimental observable in cw absorption spectroscopy. The stochastic operator Γ accounts for the ongoing tumbling motion of the particle due to interactions with the surrounding medium, but is not allowed to induce transitions between spin or nuclear-spin states ($[\Gamma,\mathbf{S}]=[\Gamma,\mathbf{I}]=0$). Since both the Hamiltonian and the stochastic operator Γ conserve the spin quantum number, the density matrix ρ must be a linear combination of elementary matrices with definite in- and outgoing spin quantum numbers:

$$|m'\rangle\langle m|\otimes\hat{\rho}_{m'm}(t,\Omega)\ , \tag{8}$$

where the reduced density matrices $\hat{\rho}_{m'm}$ have components in nuclear-spin space only. Expansion of the SLE on this basis leads to a separate equation for the reduced density matrix of each individual spin quantum pair (m',m):

$$\dot{\hat{\rho}}=\frac{i}{2\hbar}((m-m')\{\hat{\rho},\hat{H}\}+(m+m')[\hat{\rho},\hat{H}))-\Gamma\hat{\rho}+2\kappa\langle m'|S_x|m\rangle\cos\omega_0 t\ , \tag{9}$$

where we suppressed the subscripts m',m for notational simplicity. According to the classification of Ref. [14], Eq. (9) is an example of an inhomogeneous multiplicative stochastic differential equation. It constitutes a set of coupled equations for $(2I+1)^2$ complex quantities for each individual pair (m',m). Only for the special case where the hyperfine coupling is isotropic [$A(\Omega)=\text{const}\times 1$] the nuclear-spin quantum number is conserved as well and complete factorization of Eq. (9) occurs. In the following we will only consider the anisotropic case. From inspection of the harmonic driving term it is clear that only terms with spin quantum numbers satisfying $m'=m\pm 1$ are being driven by the microwave field. Precisely these components contribute to the transverse magnetization $M_x=\hbar\,\mathrm{tr}\rho S_x$ which is detected in a typical absorption experiment. The driving strength depends on the spin value S through

$$\langle m\pm 1|S_x|m\rangle=\tfrac{1}{2}\sqrt{(S\mp m)(S\pm m+1)}\ . \tag{10}$$

Interestingly, this is the only location where dependence on S enters the equations. We observe that the reduced equation of motion contains both commutators and anticommutators. This indicates that no preservation of Hermiticity or probability will occur for individual reduced density matrices $\hat{\rho}$. Instead, the components with other (m',m) quantum numbers have to be considered as well to retrieve the usual Hermiticity and preservation of trace for the full density matrix.

The reduced equation of motion Eq. (9) may be solved rigorously for several spin nuclear-spin combinations using a stochastic operator of separable form. In the next section we treat the case of a spin-$\frac{1}{2}$ hyperfine doublet. While the essentials of this problem were already presented in Ref. [15], we here give a more elaborate discussion of the algebraic details and the physical aspects of the solution. This will facilitate the subsequent investigation of the dynamical singularities in the line-shape function.

III. THE CASE $S=\frac{1}{2}, I=\frac{1}{2}$

With $\mathbf{S}=\frac{1}{2}\boldsymbol{\sigma}$, $\mathbf{I}=\frac{1}{2}\boldsymbol{\sigma}$ and $\boldsymbol{\sigma}$ the usual Pauli matrices, the equation of motion for the positive helicity component $(m'=\frac{1}{2},m=-\frac{1}{2})$ takes the form [cf. Eq. (9)]

$$\dot{\hat{\rho}}=\frac{-i}{2\hbar}\{\hat{p},\hat{H}\}-\Gamma\hat{\rho}+\kappa\cos\omega_0 t\ . \tag{11}$$

The second driven component with negative helicity $(m'=-\frac{1}{2},m=\frac{1}{2})$ obeys the complex-conjugate equation.

In what follows we will only consider the $e^{-i\omega_0 t}$ component in the harmonic driving term, since we are in the linear-response regime where the omitted contribution may be constructed by changing the sign of the frequency.

These equations may be solved in closed form with the simplest rank-one separable choice [16] for the stochastic operator Γ

$$\Gamma=\tau^{-1}(1-\Pi_0)\ . \tag{12a}$$

Here Π_0 stands for the operator which averages over all Euler angles of the particle:

$$\Pi_0=\frac{1}{8\pi^2}\int d\Omega\ , \tag{12b}$$

which is characterized by monotonic decay towards the isotropic stationary distribution. This decay is governed by a single decay time constant τ. This operator may be extended to account for considerably more complicated dynamical processes as well [11].

The commutator algebra of Eq. (11) is simplified considerably by expanding the reduced density matrix on the basis of the Pauli matrices plus the unit matrix $\{\sigma\}\cup\{1\}$. We therefore associate each 2×2 matrix $\hat{\rho}$ with a complex four-component quantity Φ:

$$\hat{\rho}=\boldsymbol{\rho}\cdot\boldsymbol{\sigma}+\rho_4\times\underline{1}\Longrightarrow(\boldsymbol{\rho},\rho_4)\equiv\Phi\ . \tag{13}$$

Due to the anticommutator identity for Pauli matrices $\{\sigma_i,\sigma_j\}=2\delta_{ij}$ the Fourier transform of Eq. (11) takes the form of an algebraic vector equation

$$(\Delta-iD)\Phi=\tau^{-1}\overline{\Phi}+\frac{\kappa}{2}\hat{\mathbf{e}}_4\ , \tag{14}$$

where $\hat{\mathbf{e}}_4\equiv(0,1)$, $\overline{\Phi}\equiv\Pi_0\Phi$, and $\Delta\equiv i\omega(\Omega)-i\omega_0+\tau^{-1}$. The operator D introduces coupling between various components and is of dyadic form

$$D=\tfrac{1}{2}(\hat{\mathbf{e}}_4\mathbf{a}+\mathbf{a}\hat{\mathbf{e}}_4)=\frac{1}{2}\begin{pmatrix} & & & a_x\\ & \underline{0} & & a_y\\ & & & a_z\\ a_x & a_y & a_z & 0\end{pmatrix}, \tag{15}$$

where we identify $\mathbf{a}=(\mathbf{a}(\Omega),0)$ in an obvious way. Algebraic solution of Eq. (14) requires computation of the resolvent, i.e., the inverse of the complex 4×4 matrix $\Delta-iD$. This resolvent necessarily has the form of a linear combination of 1, D, and D^2 as higher powers of D are reducible due to its dyadic character. Solving for the coefficients, we find the resolvent:

$$(\Delta-iD)^{-1}=\Delta^{-1}+\frac{iD}{\Delta^2+a^2/4}-\frac{D^2}{\Delta(\Delta^2+a^2/4)}\ . \tag{16}$$

A closed algebraic equation for $\overline{\Phi}$ is subsequently obtained by application of the angular-averaging operator Π_0. Conveniently, the equations for the first two components of $\overline{\Phi}$ turn out to decouple as the angle averaging reduces the full four-component problem to a $1\oplus 1\oplus 2$ set of algebraic equations:

$$\bar{\Phi}=\begin{bmatrix} g_0 & 0 & & \\ 0 & g_0 & \underline{0} & \\ & & g_1+g_3 & ig_2 \\ & \underline{0} & ig_2 & g_1 \end{bmatrix}(\tau^{-1}\bar{\Phi}+\frac{\kappa}{2}\hat{\mathbf{e}}_4) , \tag{17}$$

$$g_0\equiv\Pi_0\Delta^{-1}-\tfrac{1}{2}g_3,\quad g_1\equiv\Pi_0\frac{\Delta}{\Delta^2+a^2/4} ,$$
$$g_2\equiv\Pi_0\frac{a_z/2}{\Delta^2+a^2/4},\quad g_3\equiv\Pi_0\frac{(a^2-a_z^2)/4}{\Delta(\Delta^2+a^2/4)} , \tag{18}$$

In most cases, one is interested in electron-spin observables which require the trace over the nuclear-spin degrees of freedom (for example, absorption or spin-echo spectroscopy). As only the fourth component of $\bar{\Phi}$ survives under this trace, the desired amplitudes are located in the two-dimensional subspace spanned by $\hat{\mathbf{e}}_3\oplus\hat{\mathbf{e}}_4$. Hence they may be solved algebraically by inversion of a 2×2 matrix. The cw power absorption $P(\omega_0)$, for instance, is found as the sum of the positive and negative helicity components

$$\begin{aligned} P(\omega_0)&\sim\hbar\omega_0\kappa\hat{\mathbf{e}}_4\cdot[\bar{\Phi}(\tfrac{1}{2},-\tfrac{1}{2})+\bar{\Phi}(-\tfrac{1}{2},\tfrac{1}{2})] \\ &=\hbar\omega_0\kappa 2\,\mathrm{Re}\,\hat{\mathbf{e}}_4\cdot\bar{\Phi}(\tfrac{1}{2},-\tfrac{1}{2}) \\ &=\hbar\omega_0\kappa^2\,\mathrm{Re}\frac{g_1-d/\tau}{1-\dfrac{2g_1+g_3}{\tau}+d/\tau^2} , \end{aligned} \tag{19}$$

where $d\equiv g_1(g_1+g_3)+g_2^2$ is the discriminant of the 2×2 submatrix in Eq. (17). This exact line-shape formula has a variety of applications. First it provides predictions for microwave absorption spectra of hyperfine doublets. (cf. Ref. [15] for this application to a realistic nitroxide doublet). Moreover, imposing proper initial conditions, the Fourier transform of the response function may be used to describe the propagation of the transverse magnetization in real time, as is required for time-resolved spectroscopy. In the latter case longitudinal components of the magnetization will generally be needed as well (as, for example, in longitudinally detected electron spin resonance, spin-echo spectroscopy with nonideal pulse shapes, or measurements of longitudinal relaxation times). This requires consideration of the reduced matrices with $(m'm)=(\frac{1}{2},\frac{1}{2})$ and $(-\frac{1}{2},-\frac{1}{2})$ spin quantum pairs as well. For completeness, we quote the associated equation of motion:

$$\dot{\hat{\rho}}(m'=m)=\frac{i}{\hbar}m[\hat{\rho},\hat{H}]-\Gamma\hat{\rho} . \tag{20}$$

It is mathematically equivalent to the damped anisotropic Zeeman precession of a spin-$\frac{1}{2}$ particle in a static magnetic field. We do not pursue that direction in this paper further, but just remark that this problem may be solved in closed form as well. As a final application, the angle-averaged density matrices $\bar{\Phi}$ may be resubstituted into Eq. (14) to reconstruct the complete angle dependence of the density matrix itself. The latter procedure is required for evaluation of orientation-dependent observables as they arise in optical spectroscopy, for example. In what follows, however, we will restrict ourselves to a closer consideration of the basic absorption line shape as given by Eq. (19).

IV. THE CASE $S=1$, I ARBITRARY

As a second application of the reduced equation of motion we will consider a spin-triplet system with hyperfine coupling. Historically, this system is relevant for the simulation of absorption spectra of biradical spin probes. In principle, the high sensitivity of such spectra for microscopic orientational order makes these stable compounds the spin probes of choice for structural studies [17] in liquid crystals or lipid membranes. In practice, widespread application has been hampered by technical difficulties associated with the synthetization chemistry and purification (for a review cf. Ref. [18]). In the past years, however, the progress in time-resolved spectroscopy has greatly increased the interest in transient-spin-triplet systems. The latter not only have crucial importance for photochemical studies, but also afford excellent experimental sensitivity. The latter results from the large spin polarizations [19] induced in photoexcited systems by spin-selective intersystem crossing (ISC) or chemically induced electron polarization (CIDEP). These typically exceed thermal-equilibrium Boltzmann polarizations by several orders of magnitude.

As it turns out, the reduced equation of motion assumes a very simple form for electron spin $S=1$. The tranverse components of the magnetization now involve four spin quantum pairs $(m',m)=(1,0)$, $(0,-1)$, $(0,1)$, and $(-1,0)$. In what follows we will only consider the positive helicity amplitude with $(m',m)=(1,0)$. From this amplitude the final three may be constructed by Hermitian conjugation or time reversal. The equation of motion for the (1,0) pair is found from Eq. (9):

$$\dot{\hat{\rho}}=\frac{-i}{\hbar}\hat{H}\hat{\rho}-\Gamma\hat{\rho}+\sqrt{2}\kappa\cos\omega_0 t . \tag{21}$$

The square-root strength factor derives from Eq. (10). As in the $S=\frac{1}{2}$ case, we proceed by Fourier transform to frequency space and the rotating-wave truncation $2\kappa\cos\omega_0 t\Longrightarrow\kappa e^{-i\omega_0 t}$. Being Hermitian, the reduced Hamiltonian may be diagonalized by a unitary transformation S. Technical details of a suitable choice for S have been given in Appendix A.

In frequency space, the equation of motion is (denoting the Fourier transform of $\hat{\rho}$ with ρ, and $a=|\mathbf{a}|$)

$$S(\Delta-iaI_z)S^{\dagger}\rho=\tau^{-1}\bar{\rho}+\kappa/\sqrt{2} . \tag{22}$$

Except for frequencies on the usual cuts $\Delta=i\mu a$ $(\mu=-I,\ldots,+I)$ the left-hand side operator has an inverse T (usually called the resolvent)

$$T=S(\Delta-iaI_z)^{-1}S^{\dagger} . \tag{23}$$

A closed algebraic equation for $\bar{\rho}$ is subsequently obtained by application of the angular-averaging operator Π_0. As explained in Appendix A, this angle average renders T in a diagonal form:

$$\bar{T}\equiv\Pi_0 T=\sum_{\mu}|\mu\rangle\bar{T}_{\mu}\langle\mu| , \tag{24}$$

where μ runs over the eigenvalues of I_z. As a direct corollary, we find that the reduced density matrix $\bar{\rho}$ must be diagonal in nuclear-spin space as well. Its solution is easily found:

$$\bar{\rho}=(\kappa/\sqrt{2})\sum_{\mu}|\mu\rangle\frac{\bar{T}_{\mu}}{1-\tau^{-1}\bar{T}_{\mu}}\langle\mu| \ . \tag{25}$$

From this relation the full angle dependence of ρ may be reconstructed explicitly using

$$\rho(\Omega)=T(\Omega)(\tau^{-1}\bar{\rho}+\kappa/\sqrt{2}) \ , \tag{26}$$

which is seen to have off-diagonal elements as well.

The total power absorption $P(\omega_0)$ is found by adding contributions from all spin quantum pairs which are driven by the transverse microwave field and taking the trace over the nuclear-spin states:

$$\begin{aligned}P(\omega_0)&\sim\hbar\omega_0\kappa\,\mathrm{tr}_I\frac{1}{\sqrt{2}}[\bar{\rho}(1,0)+\bar{\rho}(0,-1)+\bar{\rho}(0,1)\\&\qquad+\bar{\rho}(-1,0)]\\&=\hbar\omega_0\kappa\,\mathrm{tr}_I\frac{4}{\sqrt{2}}\,\mathrm{Re}\,\bar{\rho}(1,0)\\&=\hbar\omega_0\kappa^2\,\mathrm{Re}\sum_{\mu}\frac{\bar{T}_{\mu}}{1-\tau^{-1}\bar{T}_{\mu}} \ .\end{aligned} \tag{27}$$

This line-shape function has an interesting analytical structure under conditions of fast modulation. The dynamical poles located on the physical sheet may be investigated with the methods of the Appendix in Ref. [11]. After choosing a closed contour running along the branch cuts and encircling the upper half of the physical plane, the number of poles in the response function is given by the winding number of the denominator around zero. Every individual $\bar{T}_{\mu}$ has $2I+1$ branch cuts in the complex plane, each with a non-negative spectra density. Since these cuts are disjoint, each cut produces at least one loop of $\bar{T}_{\mu}$ in the complex plane. Therefore the equation $1-\tau^{-1}\bar{T}_{\mu}=0$ must have at least $2I+1$ solutions under conditions of fast modulation. The precise number depends on the detailed properties of the spectral densities over the cuts. This implies the presence of at least $(2I+1)^2$ poles in the full line-shape function (barring accidental degeneracy). This abundance of poles must be located between the branch cuts and the real axis, as demanded by causality. A subset of $2I+1$ of these resides close to the real axis (the so-called Redfield poles), whereas the rest stay very close to the distant branch cuts. These non-Redfield poles soon leave the physical plane as the correlation time τ is increased. This unexpected behavior becomes clear by shifting the contour used for counting the dynamical poles in the physical plane. As soon as the contour is shifted away from the cuts over a distance of about the separation between the branch points of adjacent cuts, each individual function $\bar{T}_{\mu}$ will trace out only a single resonant loop in the complex plane as its argument runs along the test contour. This implies that the shifted contour now encloses a single isolated pole only, i.e., the Redfield pole. All the other, non-Redfield poles must therefore lie outside of the contour. By implication, they must lie close to the cuts, and only reside on the physical plane for very short correlation times. Since under such conditions the cuts are located far away from the real axis, the same must hold for the non-Redfield poles also. Each individual $\bar{T}_{\mu}$ is seen to provide at least $2I$ of such remote poles. For the full line-shape function this implies the interesting situation of the existence of at least $2I(2I+1)$ singularities in the physical plane which are never observable.

In the next section we will apply the line-shape formula to $S=1$ hyperfine doublets and triplets, and study the effects caused by a number of approximations.

V. TEST OF APPROXIMATIONS

Apart from being useful for the analysis of experimental data, the exact line-shape formulas Eqs. (14) and (27) may be used to investigate the merits of certain approximations which are often found in the literature. In this work we will study three prescriptions: The Redfield approximation (RA), the pseudosecular approximation (PSA), and the modulus approximation (MA).

The first, RA, is most widely used and valid for short correlation times (of the multitude of discussions c.f., eg., Ref. [20]). The relevant expressions for our problem are derived in Appendix B. In contradistinction, the PSA and MA do not impose conditions on the correlation time but rigorously account for the stochastic dynamics. Instead, they apply a truncation which renders the reduced Hamiltonian $\hat{H}$ diagonal in nuclear-spin space [cf. Eq. (4)]:

$$\hat{H}=\begin{cases}\hbar[\omega(\Omega)-\mathbf{a}\cdot\mathbf{I}] & \text{(Exact)}\\ \hbar[\omega(\Omega)-a_zI_z] & \text{(PSA)}\\ \hbar[\omega(\Omega)-|\mathbf{a}|I_z] & \text{(MA)} \ .\end{cases} \tag{28}$$

In the following we will use the term "diagonalizing approximation" for both PSA and MA. For isotropic hyperfine couplings, the three forms of Eq. (28) are equivalent. For anisotropic couplings the PSA is expected to be reliable for short correlation times where pseudosecular terms $\sim I_x, I_y$ will be averaged out by the fast modulation process. The MA, on the other hand, is expected to be reliable in the rigid limit, where the correlation time τ tends to infinity. Both PSA and MA lead to reduced density matrices $\hat{\rho}$ which are diagonal in nuclear-spin space themselves. Their angle averages $\Pi_0\hat{\rho}$ may be easily solved from Eq. (9). For a positive helicity component $m'=m+1$ we find the line-shape function, valid for both diagonalizing approximations and arbitrary spin:

$$\Pi_0\hat{\rho}=\kappa\langle m+1|S_x|m\rangle\sum_{\mu=-I}^{I}|\mu\rangle\frac{Q_{\mu}}{1-\tau^{-1}Q_{\mu}}\langle\mu| \ , \tag{29}$$

where we defined

$$Q_{\mu}\equiv\Pi_0\frac{1}{\Delta-i\mu\chi} \tag{30}$$

and $\chi\equiv a_z$ for PSA, and $\chi\equiv a=|\mathbf{a}|$ for MA. For spin $\frac{1}{2}$, this formula is markedly different from the exact result

TABLE I. Positions of the dynamical poles λ_1 and λ_2 for $S=\frac{1}{2}$, $I=\frac{1}{2}$ as a function of correlation time τ (in ns). Pole positions are shown in $f=\omega/2\pi$ space and taken relative to the center X-band frequency. The top and bottom halves of the table give, respectively, the high- and low-frequency poles λ_1 and λ_2 in MHz. The numerical parameters and the meaning of the approximations are given in Sec. V.

τ	Exact	RA	PSA	MA
0	(30.5,0.0)	(30.5,0.0)	(30.5,0.0)	(36.0,0.0)
1	(30.6,−1.80)	(30.5,−1.81)	(30.5,−0.63)	(35.9,−0.72)
2	(31.1,−3.49)	(30.4,−3.62)	(30.4,−1.26)	(35.9,−1.43)
3	(31.8,−5.01)	(30.3,−5.42)	(30.3,−1.89)	(36.0,−2.16)
4	(32.5,−6.30)	(30.1,−7.20)	(30.2,−2.51)	(36.1,−2.90)
5	(33.3,−7.43)	(29.9,−8.96)	(30.1,−3.11)	(36.2,−3.65)
0	(−30.5,0.0)	(−30.5,0.0)	(−30.5,0.0)	(−36.0,0.0)
1	(−30.3,−4.25)	(−30.5,−4.24)	(−30.4,−3.05)	(−35.8,−3.20)
2	(−29.7,−8.61)	(−30.4,−8.48)	(−29.4,−6.04)	(−35.3,−6.49)
3	(−28.3,−13.1)	(−30.3,−12.7)	(−28.0,−8.83)	(−34.5,−9.89)
4	(−25.5,−17.6)	(−30.1,−17.0)	(−25.9,−11.2)	(−33.2,−13.5)
5	(−20.7,−20.7)	(−29.9,−21.3)	(−23.5,−12.9)	(−31.0,−17.1)

Eq. (19), except for large values of the correlation time, where the exact response function reduces to the MA result: $g_1=\frac{1}{2}(Q_+ + Q_-)$. For spin 1, at first sight the approximate formula closely resembles the exact expression in Eq. (27) provided the Q_μ are good approximations for the $\bar{T}_\mu$. But this cannot be the case, as the former contain a single branch cut only, whereas each individual $\bar{T}_\mu$ contains all $2I+1$ cuts.

This is a clear warning that any approximation may drastically affect the analytical structure of the response function in the complex frequency plane. The Redfield approximation, for example, completely removes the branch cuts which dominate the line-shape formulas under conditions of slow modulation. The diagonalizing approximations, on the other hand, suppress the coupling between the individual transitions within the multiplet. These two approximations therefore remove the cluster of non-Redfield poles which is known to exist far from the real axis under conditions of fast modulation.

After these general remarks let us turn to numerical results for the case $S=\frac{1}{2}$, $I=\frac{1}{2}$. For a realistic doublet the diagonal elements of the coupling matrices g_d and A_d were taken to be (2.0081, 2.0024, 2.0061) and (−10, −47, −8.3) G, parameters which are representative [21] for a ^{15}N ($I=\frac{1}{2}$) nitroxide spin probe. Absorption line-shape predictions for this case were given in Ref. [15]. For a meaningful comparison of the approximations we concentrate on the singularities which lie closest to the real axis. Under conditions of fairly fast modulation ($\Delta\omega\tau\leq 1$) dynamical poles are known to exist on the encircled Riemann sheet. Their positions are fully determined by the correlation times of the modulation process itself.

Numerical evaluation of the line-shape formulas was done as follows. The angle averaging operator Π_0 involves integration over the Euler angles. Whereas the α integration could be done analytically in closed form, the remaining angular integrals were implemented numerically with a standard Gaussian integration. Care must be taken for the branch cuts which are located at $\Delta=\pm i\mu\chi$. As long as these singularities remain separated from the frequency point under consideration by more than 6 MHz, adequate numerical accuracy is obtained with 16-point Gaussian meshes for both β and γ integration. In particular, no subtraction was required to deal with the branch-cut singularities. The positions of the dynamical poles were evaluated with a standard search routine as well as by integration along properly chosen closed contours. A six-point integration around a circular contour was used. The methods yielded coinciding results. Moreover, the integration method furnished the crucial additional information that no dynamical singularities exist in the encircled region other than the two dynamical poles (as explained in Ref. [11], the precise number of poles is closely related to the form of the discontinuity over the cut).

For a given reduced density matrix $\hat{\rho}$, the (complex) residue R of a particular singularity (pole or cut) is defined as

$$R=\frac{1}{2\pi}\oint_\gamma d\omega\,\Pi_0\,\mathrm{tr}_I\hat{\rho}\,, \tag{31}$$

where γ is a closed contour encircling that and only that singularity counterclockwise, and the trace is taken over the nuclear degrees of freedom. We normalize the response functions such that the sum of all residues (poles and cuts) adds up to unity.

The results of these calculations are presented in Tables I and II, which show the positions and residues of the two dynamical poles, respectively, for correlation times up to 5 ns. For still longer correlation times the branch cuts have come so close to the real axis that the pole characteristics cannot be considered a meaningful representation of the actual line shape. The real part of the spectral distance between the two poles is equivalent

TABLE II. Residues of the dynamical poles for $S=\frac{1}{2}$, $I=\frac{1}{2}$ as a function of the correlation time τ (in ns). The complex residues are defined as in Eq. (31). The top and bottom halves of the table give the residues of the high- and low-frequency poles, respectively.

τ	Exact	RA	PSA	MA
0	(0.50,0.0)	(0.50,0.0)	(0.50,0.0)	(0.50,0.0)
1	(0.51,−0.02)	(0.50,−0.02)	(0.50,0.0)	(0.50,0.0)
2	(0.54,−0.03)	(0.50,−0.04)	(0.51,0.0)	(0.51,0.0)
3	(0.58,−0.03)	(0.49,−0.06)	(0.52,0.0)	(0.52,0.0)
4	(0.62,−0.01)	(0.49,−0.08)	(0.53,−0.01)	(0.54,0.0)
5	(0.66,0.01)	(0.48,−0.09)	(0.55,−0.01)	(0.56,0.0)
0	(0.50,0.0)	(0.50,0.0)	(0.50,0.0)	(0.50,0.0)
1	(0.52,0.02)	(0.50,0.02)	(0.51,0.0)	(0.51,0.0)
2	(0.57,0.05)	(0.50,0.04)	(0.54,0.01)	(0.54,0.01)
3	(0.67,0.13)	(0.51,0.06)	(0.57,0.05)	(0.60,0.03)
4	(0.78,0.33)	(0.51,0.08)	(0.60,0.12)	(0.68,0.09)
5	(0.66,0.65)	(0.52,0.09)	(0.60,0.20)	(0.78,0.22)

to the doublet line splitting, and is shown in Fig. 1.

It is obvious that the MA fails for both location and distance to the real axis. The systematic and severe overprediction of the line splittings can be understood from the fact that the MA uses the full length of the hyperfine vector **a** [cf. Eq. (28)]. At the same time, this overemphasis on large effective hyperfine splittings leads to an underestimate of the linewidths (i.e., the distance between pole and real axis). For the PSA, on the other hand, the line splittings are slightly underestimated, but satisfactorily follow the correlation-time dependence of the exact calculation. The general trend of rising residues for both poles is also retained in this approximation. Turning to linewidth predictions, we observe that the omission of the pseudosecular terms brings the dynamical poles too close to the real axis, resulting in a linewidth reduction by a factor of up to $2\frac{1}{2}$. In contrast, the RA accurately predicts the pole position for correlation times up to 2 ns ($\Delta\omega t\approx 0.4$), far beyond the expected range of validity. For longer correlation times, it fails to reproduce either the reduction in line splitting or the increase in residues found in the exact calculation. This feature is typical for the Redfield approach as it is caused by the removal of the branch cuts. It may be understood from the fact that the response function was normalized to unit residue for a contour encircling all singularities in the physical plane (poles and cuts). As the Redfield poles are the only singularities surviving under the RA, their residues necessarily add up to unity. In contradistinction, the sum of pole residues easily exceeds unity for the other three calculations, the compensating spectral weight being located in the cuts. At $\tau=5$ ns, the latter have come to within 32 MHz spectral distance from the real axis, and therefore may not be neglected anymore.

With view to applications in time-resolved spectroscopy, an interesting quantity to consider is the effective phase-memory time T_2^*, defined as the inverse distance between the real axis and the nearest singularity in frequency space. In a simple Hahn echo experiment, for example, this quantity determines the decay of the echo amplitude with increasing time interval between the pulses. The results are shown in Fig. 2. The plot for the exact calculation (solid line) may be visualized as follows. For small correlation times, the closest singularity is the dynamical pole λ_1, which moves away from the real axis as the correlation time increases. At a critical correlation time $\tau_c\approx 11.5$ ns, this pole meets the approaching branch cut and slips onto the second Riemann sheet. The branch cuts now are the only singularities left in the physical region and all have the same distance τ^{-1} to the real axis. This implies the identity $T_2^*=\tau$ for $\tau>\tau_c$. We thus find that the phase-memory time increases without bound for both very small and very long correlation times. In the intermediate region it exhibits a pronounced minimum.

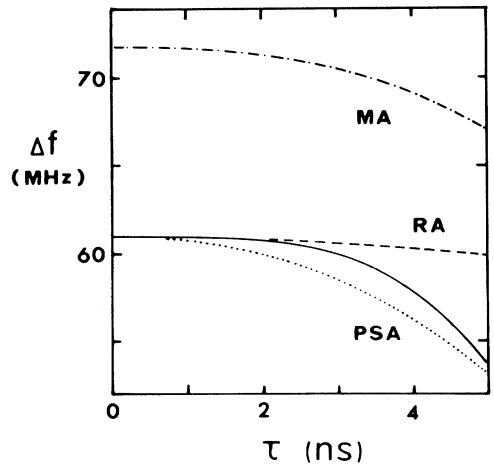

FIG. 1. $S=\frac{1}{2}$, $I=\frac{1}{2}$ line splitting $\Delta f=\mathrm{Re}(\lambda_1-\lambda_2)$ as a function of the correlation time τ. The solid curve gives the exact calculation. The other curves show the effects of the approximations of Sec. IV.

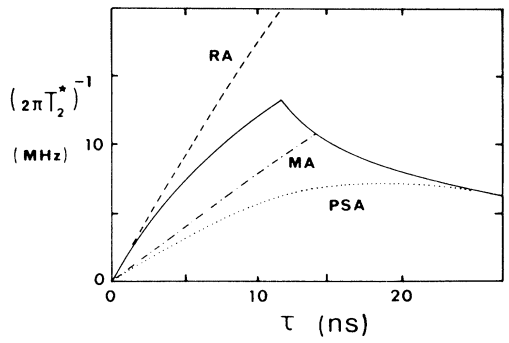

FIG. 2. Effective phase-memory time T_2^* for $S=\frac{1}{2}$, $I=\frac{1}{2}$ as a function of the correlation time τ. $(2\pi T_2^*)^{-1}$ is the distance in $f=\omega/2\pi$ space between the real axis and the nearest singularity of the response function. The labeling of the lines corresponds to that of Fig. 1. After intersection, the MA and PSA follow the trajectory of the exact calculation (solid curve).

This behavior shows that the critical correlation time τ_c plays three important roles in the current model. First and foremost, it is the correlation time at which the last remaining dynamical pole leaves the physical sheet. Second, it is the absolute lower bound for the phase-memory time. Finally, it is the value of the correlation time at which the phase-memory time reaches this minimum.

Since the diagonalizing approximations do not affect the location of the branch cuts, both PSA and MA trajectories intersect the exact curve. The critical correlation times for this to happen depends on the spectral densities of the cuts, and therefore on the approximation used. In all cases the derivatives of the curves exhibit a discontinuity at the intersection. Since the branch cuts are seen to be responsible for the increase in T_2^* when modulation becomes slow, it is not surprising that this behavior is completely absent from the calculation in the Redfield approximation.

Returning to the line shape, we just mention that, for progressively longer correlation times $\tau > \tau_c$, the MA becomes an increasingly better approximation, whereas RA and PSA produce severe overestimates and underestimates, respectively, of the linewidths. These results may be compared with previous calculations [22] in an eigenvalue approach using Brownian diffusion dynamics instead of the separable operator Eq. (12). For axially symmetric couplings, the Brownian model was able to predict line shapes over a wide range of correlation times, and reported strong effects of the PSA on the predicted line shapes. Our results confirm these conclusions. Moreover, we found that the observed effects are caused by the coupling between the individual transitions within the multiplet. A further advantage of our model is the validity of our analytical response function for fully anisotropic couplings. The latter would require a substantial increase in the dimension of the matrix employed in the eigenvalue approach. Such complications greatly enhance the reported [9] numerical problems concerning the positions and weights of the line-shape singularities. This is probably of minor importance for pure absorption spectroscopy under conditions of fast or intermediate modulation, as witnessed by an abundance of experimental literature with excellent line-shape simulations based on the eigenvalue approach. They do matter, however, under conditions of slow modulation, and in particular for applications to time-resolved spectroscopy. In this case precise knowledge of the singularities is required for the evaluation of the contour integrals associated with the propagation in time of the magnetization. These remarks conclude our discussion of the case $S=\frac{1}{2}$, $I=\frac{1}{2}$, and we turn to spin-triplet response functions.

First, we quickly consider the hyperfine doublet. At first sight, the overall lineshape resembles the previous $S=\frac{1}{2}$, $I=\frac{1}{2}$ case, in particular under conditions of slow modulation (the two line shapes coincide in the rigid limit). However, closer inspection reveals an interesting discrepancy in the dynamical behavior for short correlation times, as the line splitting now is seen to increase with the correlation time up to around 3 ns (cf. Fig. 3). This particular feature is significant, since the predictions

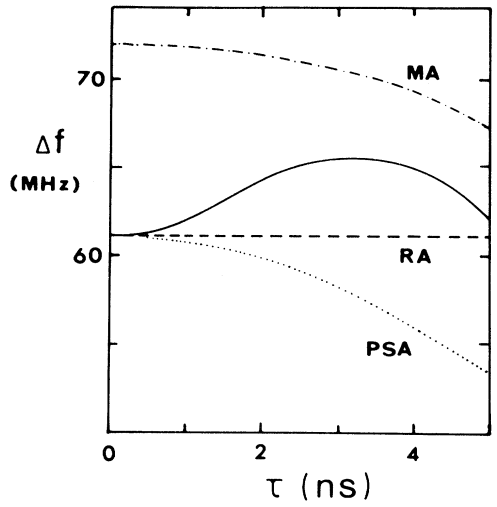

FIG. 3. $S=1$, $I=\frac{1}{2}$ line splitting as a function of correlation time τ. The magnetic coupling parameters and curve labeling are identical to those of Fig. 1.

from the two diagonalizing approximations are identical for the $S=\frac{1}{2}$ and 1 case. We conclude that the seemingly correct line-splitting predictions in the $S=\frac{1}{2}$ PSA were accidental and not related to the underlying dynamics of the full problem. We also note that in the case of RA, the line splitting has lost any correlation-time dependence. This is a direct reflection of the fact that in the $S=1$ calculation the Redfield relaxation matrix R_0 assumes diagonal form, whereas for $S=\frac{1}{2}$ off-diagonal terms remain.

We now turn our attention to the $S=1$ hyperfine triplet. The line-shape predictions from Eq. (27) are shown in Fig. 4 for three different correlation times τ. The diagonal elements of the coupling matrices were chosen as $g_d=(2.0081,2.0024,2.0061)$ and $A_d=(5.6,34.0,5.3)$ G. As such it mimics an idealized ^{14}N ($I=1$) biradical with perfect alignment of the two nitroxide groups, and where spin-spin interactions between the groups are neglected. (Realistic biradicals usually exhibit large zero-field splittings, indicating that intramolecular spin-spin interactions should be taken into account. While our model does admit such extensions, our concern in this paper is restricted to spin-triplet spectroscopy.) With the above choice of hyperfine anisotropy, strong effects of the molecular motion on the absorption line shape can be expected for correlation times near 5 ns, as is confirmed by the collapse of the linewidths at that time scale. An interesting feature is the fact that the low field line, while very broad at slow modulation, collapses to a line which is even narrower than the central line. The physical reason is not found in the coupling between the transitions within the multiplet, but rather in the interference between the gyromagnetic and hyperfine anisotropies. Inspection of the Redfield expressions for the spin-triplet linewidths (Appendix B) shows that a calculation with isotropic gyromagnetic coupling would predict flanking lines of identical width, exceeding the central linewidth.

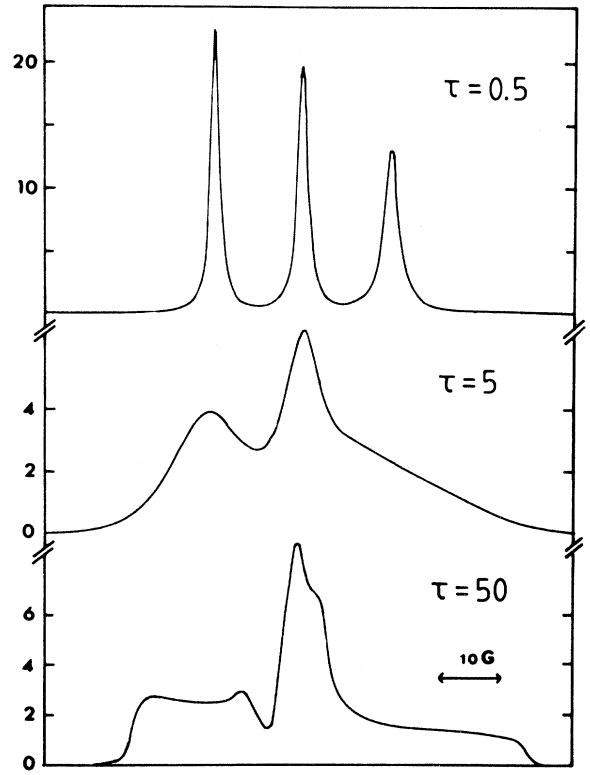

FIG. 4. X-band-absorption line shapes for $S=1$, $I=1$, computed from Eq. (27) for three rotational correlation times τ (in ns). The line-shape function is normalized to unit residue. Unit of ordinate is s/Grad.

We conclude that the narrow linewidth of the low field line results directly from the gyromagnetic anisotropy. The positions of the dynamical poles are tabulated in Table III. It shows the Redfield approximation to be effective up to correlation times of around 1 ns, which corresponds to $\Delta\omega\tau\sim 0.2$. Upon increase of the correlation time, the PSA predicts inward movement of the flanking lines, whereas both lines move to the right in the exact calculation. This feature is a manifestation of the coupling between the transitions within the multiplet. However, the total PSA splitting between the two flanking lines is satisfactory. Under the MA, the line splittings are systematically and severely overpredicted for the same reasons as in the spin-$\frac{1}{2}$ case discussed above. Turning to the linewidths, both diagonalizing approximations are seen to underpredict the distance to the real axis. Hence we obtain insufficient linewidths. This failure is particularly severe for the central line and may be easily understood from the nature of these approximations. For odd hyperfine multiplicities (integer I) the spectra exhibit a central line completely devoid of the broadening effect of the hyperfine coupling. Hence these central linewidths are determined by the gyromagnetic anistropy only, which was chosen significantly smaller than the hyperfine anisotropy in the current calculations. In applications to realistic spin-triplet spectroscopy these linewidth problems would be obviated to a large extent by the large zero-field splittings normally found in systems with an electron-spin value exceeding $\frac{1}{2}$.

VI. CONCLUSIONS

The discussion of the previous sections has demonstrated the advantages of the application of separable stochastic operators to problems with multiplicative stochastic modulation. Not only do such operators afford algebraic solutions to the equations of motion in a number of interesting cases, but they also admit a detailed study of the effects of the modulation on the linear response of the system. Of particular interest are the singularities in the response function. In all cases considered so far, these singularities are either branch cuts or simple poles. In the regime of fast modulation the response of the system is completely determined by simple poles close to the real axis, the so-called Redfield poles. Further branch cuts are located far away. The presence of coupling between internal degrees of freedom

TABLE III. Positions of the three dynamical poles for $S=1$, $I=1$ as a function of correlation time τ (in ns). The positions are shown in $f=\omega/2\pi$ space and taken relative to the center X-band frequency. Units are MHz. Parameters are given in Sec. V and differ from those of Table I. Note the severe linewidth errors caused by PSA and MA for the central line (middle section of the table). This is characteristic for multiplets with odd multiplicity.

τ	Exact	RA	PSA	MA
0	(41.9,0.0)	(41.9,0.0)	(41.9,0.0)	(50.8,0.0)
2	(43.1,−8.98)	(41.9,−9.36)	(41.4,−3.97)	(50.8,−4.47)
4	(45.4,−18.2)	(41.9,−18.7)	(39.7,−7.64)	(51.0,−9.42)
0	(0.0,0.0)	(0.0,0.0)	(0.0,0.0)	(0.0,0.0)
2	(0.11−8.43)	(0.,−11.3)	(.01,−0.55)	(.01,−0.55)
4	(−0.47,−9.96)	(0.,−22.5)	(0.06,−1.09)	(.06,−1.09)
0	(−41.9,0.0)	(−41.9,0.0)	(−41.9,0.0)	(−50.8,0.0)
2	(−39.7,−17.1)	(−41.9,−16.8)	(−39.1,−11.1)	(−49.5,−12.3)
4	(−22.9,−28.9)	(−41.9,−33.5)	(−30.7,−18.3)	(−43.6,−26.7)

produces large numbers of additional poles. Although these non-Redfield poles appear in the physical plane, they are unobservable in actual experiments as they remain in a distant region. For increasing correlation time the Redfield poles move away from the real axis, whereas the branch cuts move closer. The non-Redfield poles soon leave the physical plane by slipping through the branch cuts. Only the Redfield poles now remain. For correlation times near the typical inverse linewidth ($\Delta\omega\tau\sim 1$) the receding Redfield poles also slip through the approaching cuts. From now on the line shape is dominated by the branch cuts only and the lines in the multiplet appear severely broadened. In contrast to conventional numerical approaches, our model with separable dynamics is seen to provide a smooth and very natural scenario for the change in spectral characteristics upon transition from the Redfield to the rigid-limit regimes.

The exact solutions obtained were used to study the effects from three common approximations, the RA, PSA, and MA. All three were found to severely affect the singularity structure of the response function. The complete removal of the branch cuts in the RA proved to be most rigorous. Not surprisingly, the RA was found accurate for fast modulation but failing as soon as the effects from the branch cuts manifest themselves in the exact calculation. In the slow motional regime where no poles remain in the physical plane, the MA is clearly best, its reliability increasing with correlation time. The PSA on the other hand, predicts line-shape positions reasonably well, but fails for linewidths. This failure is most acute for multiplets with odd multiplicities: In both PSA and MA the coupling between the transitions within the multiplet is truncated. Hence the anisotropic hyperfine interactions do not broaden the central line, leaving the latter far too sharp.

In contrast to the RA, the diagonalizing approximations PSA and MA still exhibit many of the characteristic features of the exact calculation. In particular, they retain the smooth transition between Redfield and rigid-limit behavior. The reason is that the PSA and MA modify the character of the singularities in a nonessential way, namely through removal of the distant non-Redfield poles. The overall analytical character of the response function is retained, as witnessed by the unchanged location of the branch points. These desirable features are reflected in the predictions for the phase-memory time, for example. The observed changes in the overall line shape are due to the effect of these approximations on the spectral densities over the branch cuts.

To conclude, our current work has pointed out the shortcomings of a number of approximations. These results emphasize the usefulness of exact analytical results, if available. This provides a strong motivation for further application of separable dynamical models to resonant problems undergoing stochastic modulation.

APPENDIX A: STRUCTURE OF THE $S=1$ RESOLVENT OPERATOR

In Sec. IV we discussed the algebraic solution of the equation of motion for reduced density matrices for the case spin $S=1$ [cf. Eq. (21)]. This task required computation of the resolvent operator T and its angular average $\Pi_0 T$, where T^{-1} derives from the reduced Hamiltonian $\hat{H}$ in nuclear-spin space:

$$T^{-1}\equiv\frac{i}{\hbar}\hat{H}-i\omega_0+\tau^{-1}$$
$$=\Delta-i\mathbf{a}\cdot\mathbf{I}\ . \tag{A1}$$

The Hermitian character of $\mathbf{a}\cdot\mathbf{I}$ assures the existence of a unitary transformation S which under the Hamiltonian assumes diagonal form. Although not unique, the actual choice of S will not affect the final result. An explicit realization of S may be constructed in the following way. Let a denote the length of $\mathbf{a}$, and let $\mathbf{0}$ denote a rotation operator in three-dimensional space which rotates $\hat{\mathbf{e}}_z$ into the direction of $\mathbf{a}=a\hat{\mathbf{e}}_a$:

$$\hat{\mathbf{e}}_a=\mathbf{0}\hat{\mathbf{e}}_z\ , \tag{A2}$$

and let S be the representation of $\mathbf{0}$ in the nuclear-spin space. Then

$$\mathbf{a}\cdot\mathbf{I}=a(\mathbf{0}\hat{\mathbf{e}}_z)\cdot\mathbf{I}=aSI_zS^{\dagger} \tag{A3}$$

is seen to be diagonal on the basis of $S|\mu\rangle$, where $|\mu\rangle$ are the eigenfunctions of I_z. From its definition Eq. (6) we find that a depends on β and γ only [cf. Eq. (A12), below]. The operator S, on the other hand, depends on the Euler angles in a rather complicated way, in particular if the diagonal components of the hyperfine tensor do not have definite sign. However, inspection of Eqs. (2)–(6) shows that the complications are located in β and γ, whereas the dependence on α is like an elementary rotation:

$$S(\alpha,\beta,\gamma)=e^{-i\alpha I_z}\tilde{S}(\beta,\gamma)\ . \tag{A4}$$

Here the reduced unitary operator $\tilde{S}$ depends on β and γ only, albeit in a complicated way. These relations allow us to evaluate the resolvent explicitly:

$$T=e^{-i\alpha I_z}\tilde{S}(\Delta-iaI_z)^{-1}\tilde{S}^{\dagger}e^{i\alpha I_z}\ , \tag{A5}$$

where the inverse operator is well defined provided the frequency ω_0 avoids the usual cuts, defined by $\Delta=i\mu a$, $\mu=-I,\ldots,I$.

Subsequent application of the projection operator Π_0 leads to a simple form of $\Pi_0 T$, since the expression in between the exponentials of Eq. (A5) does not depend on α at all. Hence the α integration may be done at once and leads to a result which is diagonal on the basis of eigenstates $|\mu\rangle$ of I_z:

$$\Pi_0 T=\sum_{\mu}|\mu\rangle\bar{T}_{\mu}\langle\mu|\ , \tag{A6}$$

$$\bar{T}_{\mu}\equiv\Pi_0\langle\mu|\tilde{S}(\Delta-iaI_z)^{-1}\tilde{S}^{\dagger}|\mu\rangle\ , \tag{A7}$$

which proves the important Eq. (24) of Sec. IV. The complex functions $\bar{T}_{\mu}$ are explicitly given in terms of quadratures, where each individual $\bar{T}_{\mu}$ is seen to contain all $2I+1$ logarithmic cuts.

The numerical evaluation of these integrals is easiest if one parametrizes the rotation matrix $\tilde{S}$ by two new angles

ψ and φ, which are defined through the relation

$$e^{-i\varphi I_z}e^{-i\psi I_y}\equiv\tilde{S}\ . \tag{A8}$$

Since $\tilde{S}$ depends on the original Euler angles β and γ, the above relation defines a mapping $(\beta,\gamma)\rightarrow(\psi,\varphi)$. This mapping is not necessarily one to one. Expressed in these particular angles, the diagonal elements of the T matrix assume a simple form which does not depend on φ:

$$\langle\mu|\tilde{S}(\Delta-iaI_z)^{-1}\tilde{S}^{\dagger}|\mu\rangle=\sum_{\nu}\frac{\langle\mu|\tilde{S}|\nu\rangle\langle\nu|\tilde{S}^{\dagger}|\mu\rangle}{\Delta-ia\nu}$$
$$=\sum_{\nu}\frac{[d^{I}_{\mu\nu}(\psi)]^2}{\Delta-ia\nu}\ . \tag{A9}$$

We observe that each individual $\bar{T}_{\mu}$ contains $2I+1$ cuts. The spectral density over the νth cut is expressed as a square of the Wigner matrices $d^{I}_{\mu\nu}(\psi)$. The physical interpretation of this dependence of ψ is as follows. For slightly anisotropic hyperfine couplings the **a** vector nearly points in the direction on the magnetic field, irrespective of the orientation of the particle itself. This implies values of ψ close to zero. Since $d^{I}_{\mu\nu}(\psi=0)=\delta_{\mu\nu}$, the Wigner matrices will tend to suppress the $\nu\neq\mu$ cuts in $\bar{T}_{\mu}$. For increasing anisotropy the **a** vector will sweep through a wider range of directions, thereby admitting larger contributions from the $\nu\neq\mu$ components. In this way we can clearly visualize how increasing hyperfine anisotropy induces progressively stronger mixing of the individual transitions within the multiplet.

The angle-averaged quantities $\bar{T}_{\mu}$ may be computed by integrating Eq. (A9). This is a straightforward numerical procedure since the dependence on φ is lost, and the mixing angle ψ derives from the Euler angles β and γ in a simple though highly nonlinear way:

$$\cos\psi=\hat{\mathbf{e}}_a\cdot\hat{\mathbf{e}}_z=a_z/a\ , \tag{A10}$$

$$a_z=A_x\cos^2\gamma\sin^2\beta+A_y\sin^2\gamma\sin^2\beta+A_z\cos^2\beta\ , \tag{A11}$$

$$a^2=A_x^2\cos^2\gamma\sin^2\beta+A_y^2\sin^2\gamma\sin^2\beta+A_z^2\cos^2\beta\ . \tag{A12}$$

The numerical integration is potentially hazardous due to the oscillatory behavior of the Wigner matrices, as well as due to the zeros in the denominator of the integrand. The latter lead to the logarithmic branch points, which are located at a distance τ^{-1} from the real axis. For $I=1$, and $\tau<20$ ns, we found that straightforward Gaussian integration with 24 meshpoints for both β and γ variables provided adequate numerical accuracy. In particular, no subtractions of the integrand were needed.

APPENDIX B: LINE SHAPES IN REDFIELD APPROXIMATION

In most problems involving stochastic differential equations one does not require the full knowledge of the complicated dependence on the stochastic variables, but would be satisfied with knowledge of the stochastic averages $\langle\rho(t)\rangle$ as a function of time. Large efforts have therefore been devoted to suitable formulations of effective equations of motion for this stochastic average.

For problems involving multiplicative stochastic modulation, as encountered here, this reduction scheme is particularly complicated. However, in the regime of fast modulation (short correlation times), a suitable dynamical equation for $\langle\rho\rangle$ was proposed by Bourret [23] in the form of an integro-differential equation. When evaluated on time scales longer than the correlation time of the stochastic process, the Bourret equation provides the theoretical justification for the (historically older) procedure by Redfield [24]. The latter's dynamical equation for the average assumes the simple form of a first-order differential equation. When formulated in frequency space, the Bourret-Redfield analog for the $S=\frac{1}{2}$, $I=\frac{1}{2}$ equation (14) would be

$$(i\bar{\omega}-i\omega_0-i\bar{D}+\tau R_0)\bar{\Phi}=\frac{\kappa}{2}\hat{\mathbf{e}}_4\ . \tag{B1}$$

This expression only involves stochastic averages like $\bar{\Phi}\equiv\Pi_0\Phi$, etc. Up to second order in time, the effect of the stochastic modulation is taken into account via the relaxation matrix τR_0. The latter appears as the time integral of the Hamiltonian autocorrelation matrix $R(t')$:

$$\tau R_0=\int_0^{\infty}dt'R(t')\ , \tag{B2}$$

$$R(t')=\langle[\omega(\Omega_t)-D(\Omega_t)][\omega(\Omega_{t+t'})-D(\Omega_{t+t'})]\rangle\ . \tag{B3}$$

With the stochastic operator Γ as in Eq. (12) we find immediately

$$R_0=\overline{(\omega-\bar{\omega})^2}-2\overline{(D-\bar{D})(\omega-\bar{\omega})}+\overline{(D-\bar{D})^2}\ , \tag{B4}$$

where the horizontal bars denote angular averages as usual. Straightforward algebra gives

$$R_0=\begin{bmatrix}R_{11} & 0 & & \\ 0 & R_{22} & & \bar{0} \\ & & R_{33} & R_{34} \\ & \underline{0} & R_{34} & R_{44}\end{bmatrix}\ , \tag{B5}$$

$$R_{33}=\overline{\omega^2}-\bar{\omega}^2+(\overline{a_z^2}-\bar{a}_z^2)/4\ ,$$
$$R_{44}=\overline{\omega^2}-\bar{\omega}^2+(\overline{a^2}-\bar{a}^2)/4\ , \tag{B6}$$
$$R_{34}=\bar{\omega}\bar{a}_z-\overline{\omega a_z}\ .$$

The explicit dependence of these functions on the Euler angles is found as in Eqs. (A11) and (A12) of Appendix A. We note that the coupling between the third and fourth component of $\bar{\Phi}$ is preserved under the Bourret-Redfield approximation. As explained in Sec. III, the desired physical amplitude is $\hat{\mathbf{e}}_4\cdot\bar{\Phi}$ and involves the lower right submatrix of R_0 only. After inversion of the 2×2 coupling matrix, the solution of the Bourret-Redfield equation for the spin-$\frac{1}{2}$, hyperfine doublet is found to be

$$\hat{\mathbf{e}}_4\cdot\bar{\Phi}=\frac{\kappa}{2}\frac{i(\bar{\omega}-\omega_0)+\tau R_{33}}{[i(\bar{\omega}-\omega_0)+\tau R_{33}][i(\bar{\omega}-\omega_0)+\tau R_{44}]-(\tau R_{34}-i\,\bar{a}_z/2)^2}\ . \tag{B7}$$

As a function of frequency ω_0, this expression has two simple poles in the lower half plane. For increasing correlation time τ, they move away from the real axis (line broadening). The logarithmic cuts of the exact result have been lost under the Bourret-Redfield approximation. This concludes our treatment of the spin-$\frac{1}{2}$ hyperfine doublet.

Turning to the spin-1 case, the Bourret-Redfield analog for Eq. (21) is

$$(i\bar{\omega}-i\omega_0-i\,\bar{a}_z I_z+\tau R_0)\bar{\rho}=\kappa/\sqrt{2}\ . \tag{B8}$$

As before, the relaxation matrix τR_0 derives from the time integral of an autocorrelation matrix $R(t')$:

$$R(t')=\langle[\omega(\Omega_t)-\mathbf{a}(\Omega_t)\cdot\mathbf{I}][\omega(\Omega_{t+t'})-\mathbf{a}(\Omega_{t+t'})\cdot\mathbf{I}]\rangle\ . \tag{B9}$$

In contrast to the spin-$\frac{1}{2}$ case above, this autocorrelation matrix is diagonal in nuclear-spin space. Explicit evaluation of the angular integrals gives

$$\begin{aligned} R_0&=A+BI_z+CI_z^2\ ,\\ A&\equiv\overline{\omega^2}-\bar{\omega}^2+I(I+1)\overline{(a^2-a_z^2)}/2\ ,\\ B&\equiv-2(\overline{\omega a_z}-\bar{\omega}\bar{a}_z)\ ,\\ C&\equiv\overline{(3a_z^2-a^2)}/2-\bar{a}_z^2\ . \end{aligned} \tag{B10}$$

In these expressions, a_z and a^2 are again given by Eqs. (A11) and (A12). Since R_0 is diagonal, Eq. (B8) may be solved easily to yield the line-shape formula for spin 1

$$P(\omega_0)\sim\mathrm{Re}\sum_{\mu=-I}^{I}[i(\bar{\omega}-\omega_0-\mu\bar{a}_z)+\tau(A+B\mu+C\mu^2)]^{-1}\ . \tag{B11}$$

[1] S. Rytov, Y. Kravtsov, and V. Tatarskii, *Principles of Statistical Radiophysics* (Springer, Berlin, 1988).
[2] I. Fabelinskii, *Molecular Scattering of Light* (Plenum, New York, 1968).
[3] A. Abragam, *The Principles of Nuclear Magnetism* (Oxford University Press, London, 1961).
[4] H. Haken, *Laser Theory* (Springer, Berlin, 1984).
[5] P. Bordewijk and C. Böttcher, *Theory of Electric Polarization* (Elsevier, Amsterdam, 1979).
[6] A. Marek, Physica **25**, 1358 (1959).
[7] R. Kubo, J. Math. Phys. **4**, 174 (1963); J. Phys. Soc. Jpn. (Suppl.) **26**, 1 (1969).
[8] J. Norris and S. Weissman, J. Phys. Chem. **73**, 3119 (1969).
[9] G. Moro and J. Freed, J. Phys. Chem. **84**, 2837 (1980); J. Chem. Phys. **74**, 3757 (1981).
[10] G. Kothe, Mol. Phys. **33**, 147 (1977).
[11] E. van Faassen, Phys. Rev. A **42**, 2785 (1990).
[12] M. E. Rose, *Elementary Theory of Angular Momentum* (Wiley, New York, 1957).
[13] J. Freed, in *Spin Labeling,* edited by L. Berliner (Academic, New York, 1976), Vol. I.
[14] N. van Kampen, *Stochastic Processes in Physics and Chemistry* (North-Holland, Amsterdam, 1981).
[15] E. van Faassen, Phys. Rev. A **44**, 780 (1991).
[16] A. Stearn and H. Eyring, J. Chem. Phys. **5**, 113 (1937).
[17] B. Kirste, Chem. Phys. Lett. **130**, 482 (1986).
[18] G. Luckhurst, in *Spin Labeling,* edited by L. Berliner (Academic, New York, 1976), Vol. I.
[19] K. Salikhov, J. Molin, R. Sagdeev, and A. Buchachenko, *Spin Polarization and Magnetic Effects in Radical Reactions,* Vol. 22 of *Studies in Physical and Theoretical Chemistry,* edited by J. Molin (Elsevier, Amsterdam, 1984).
[20] G. Luckhurst and A. Sanson, Mol. Phys. **24**, 1297 (1972).
[21] J. Keana, S. Keana, and D. Beetham, J. Am. Chem. Soc. **89**, 3055 (1967).
[22] J. Freed, G. Bruno, and C. Polnaszek, J. Phys. Chem. **75**, 3385 (1971).
[23] R. C. Bourret, Nuovo Cimento **26**, 1 (1962).
[24] A. Redfield, IBM J. Res. Devel. **1**, 19 (1957); Adv. Magn. Reson. **1**, 1 (1966).